Interface strengthening mechanisms of Ti/CFRP fiber metal laminate after adding MWCNTs to resin matrix

Kai Jin [a,1], Hao Wang [b,1], Jie Tao [b,c,*], Xian Zhang [b]

[a] College of Mechanical and Electrical Engineering, Nanjing University of Aeronautics and Astronautics, Nanjing, 211106, PR China
[b] College of Material Science and Technology, Nanjing University of Aeronautics and Astronautics, Nanjing, 211106, PR China
[c] Jiangsu Collaborative Innovation Center for Advanced Inorganic Function Composites, Nanjing, 210016, PR China

ABSTRACT

Since the interface is the relatively weak area of fiber metal laminates (FMLs), the reinforcement of metal/resin interface is desired urgently. In this study, a metallic-inorganic-organic system and related equations were developed to describe the interfacial behaviors. The effect and mechanism of MWCNTs was analyzed under the system by using molecular dynamics (MD) simulations. Multi-walled carbon nanotubes (MWCNTs) were added to the polyimide (PI) matrix to validate the analysis result and the enhancement effect. It was found that Van der Waals force and chemical bond of MWCNTs as driven forces could improve the interface performance significantly. If laying the MWCNTs perpendicular or at 45° to the Ti surface, the interface strength would reach the maximum. The presented method could also be apply to study the graphene or other strengthening phases.

1. Introduction

Fiber metal laminates (FMLs) have widely been used in the aerospace field, where their comprehensive performance requirements should further be strengthened [1]. Ti/CFRP fiber metal laminates (abbreviated as TiGr) is designed to excellent temperature resistance, high fatigue resistance, and superior specific strength [2,3], which are made of titanium alloy sheets and carbon fiber reinforced polyimide resin prepregs. The laminates have become a potential structural material in the supersonic aircraft and fighter jets due to their excellent high-temperature performances [4].

Since the Ti layers and the CFRP layers are stacked up alternately, the strength of the metal/resin interface has a great influence on the overall performance of TiGr. To improve the bonding strength, most researches have focused on the metal surface treatment to increase roughness including mechanical processing [5], electrochemical treatment [6], coupling agent [7] and photolithography [8]. However, few researchers tried to bind the metal/resin interface through additive.

Carbon nanotubes (CNTs) based nanocomposites are expected to have superior performances due to their remarkable mechanical properties, with strength and modulus values reaching up to 150 GPa [9] and 1 TPa [10], respectively. For instance, Park and coworkers [11]

synthesized polyimide (PI) nanocomposites reinforced with single-walled carbon nanotubes (SWCNTs) through in situ polymerizations of monomers of inlunwenerest in presence of sonication. They found that mechanical, thermal, electrical and optical properties of PI were improved after incorporation of the SWCNTs. Jiang et al. [12] fabricated phenylethynyl-terminated polyimide reinforced with plasma functionalized bucky paper. Their data revealed 30% increase in tensile strength and 125% improvement in tensile modulus. Thus, PI-CNTs nanocomposites are promising candidates for fabrication of multifunctional composites with outstanding mechanical, thermal, and electrical performances. Zhang et al. [13] added different percentages of CNTs to GLARE fiber metal laminate epoxy resin layers. The measured flexural properties and low-velocity impact properties of the obtained fiber metal laminates indicated that addition of CNTs could help to increase the bending strength and bending modulus at the same time improve the impact resistance. However, they did not systematically study the mechanism of CNTs to the interface strengthening.

Due to the high cost and technical challenges of atomic level tests, it is difficult to investigate the molecular details of fiber metal laminates and Ti/PI interface at the nanoscale. Hence, the combination of molecular dynamics (MD) simulation and mesoscale or macroscale experimental verification is feasible to reveal the mechanism of interfacial

strengthening. Most molecular dynamics simulation of composite materials have been applied to a binary system [14–17] but few studies have been conducted on a ternary system such as metal-CNT-polymer system. Meanwhile, the impact of CNTs orientation on the interfacial bonding strength has rarely studied owing to the difficulty of nanoscale experiment. In this study, the effect of added MWCNTs on interfacial properties of FMLs was evaluated through MD analysis and experimental, presenting interfacial interaction energy equations of Ti-PI-MWCNTs ternary system. Meanwhile, influence of the MWCNTs orientation on the interfacial behavior were also studied.

2. Molecular dynamics analysis

2.1. Energy equations for a ternary system

In this study, a ternary was developed, including titanium, polyimide and carbon nanotube. Therefore, interfacial interaction energy equations were derived for the Ti-PI-MWCNTs system.

For the Ti-PI binary system, the cohesive energy at the interface is given by Refs. [18,19]:

$$\Delta E_{Ti\&PI} = E_{Ti-PI} - (E_{Ti} + E_{PI}) \tag{1}$$

where, $\Delta E_{Ti\&PI}$ is the cohesive energy at the interface, E_{Ti-PI} is the potential energy of the composite, E_{Ti} represents the potential energy of the Ti component, and E_{PI} is the potential energy of the PI component.

For the ternary system of Ti-PI-MWCNTs, the cohesive energy at the interface consist of three components that contact each other at the interface. The equations can be expressed by:

$$\Delta E_{Ti\&PI-MWCNTs} = E_{Ti-MWCNTs-PI} - (E_{Ti} + E_{PI-MWCNTs}) \tag{2}$$

Δ where, $\Delta E_{Ti\&PI-MWCNTs}$ denotes the cohesive energy between Ti and PI-MWCNTs, $E_{Ti-MWCNTs-PI}$ is the potential energy of the composite, $E_{PI-MWCNTs}$ is the potential energy of the PI and MWCNTs.

The effect of MWCNTs on interfacial shear behavior can be evaluated through comparing the fracture energies Gs given by Eq. (3) whether adding MWCNTs or not.
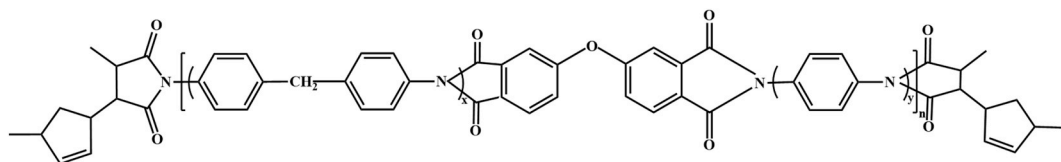
Fig. 1. The basic repeat unit of PMR (Polymerization of Monomeric Reactants) polyimide.
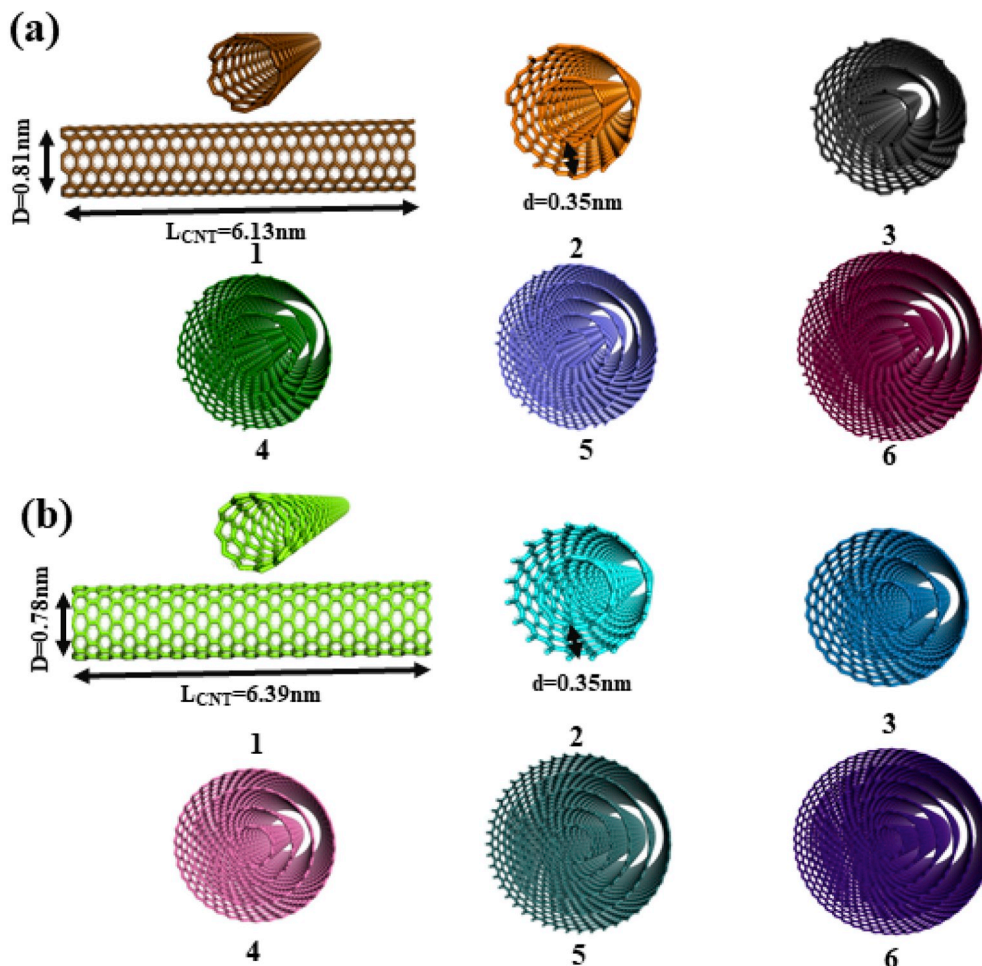
Fig. 2. CNT models: (a) Armchair (6, 6) Carbon nanotubes with different wall number; (b) Zigzag (10, 0) Carbon nanotubes with different wall number.

$$G_S = \frac{E_{max} - E_{min}}{A} \tag{3}$$

where, E_{max} is the maximum of shear total potential energy, E_{min} represents the minimum of shear total potential energy and A is the surface area.

2.2. Modeling and simulation

Molecular dynamics (MD) simulation was employed to describe the molecular-level interfacial behavior of the Ti-PI-MWCNTs ternary system. Here, interface models of titanium and polyimide with different
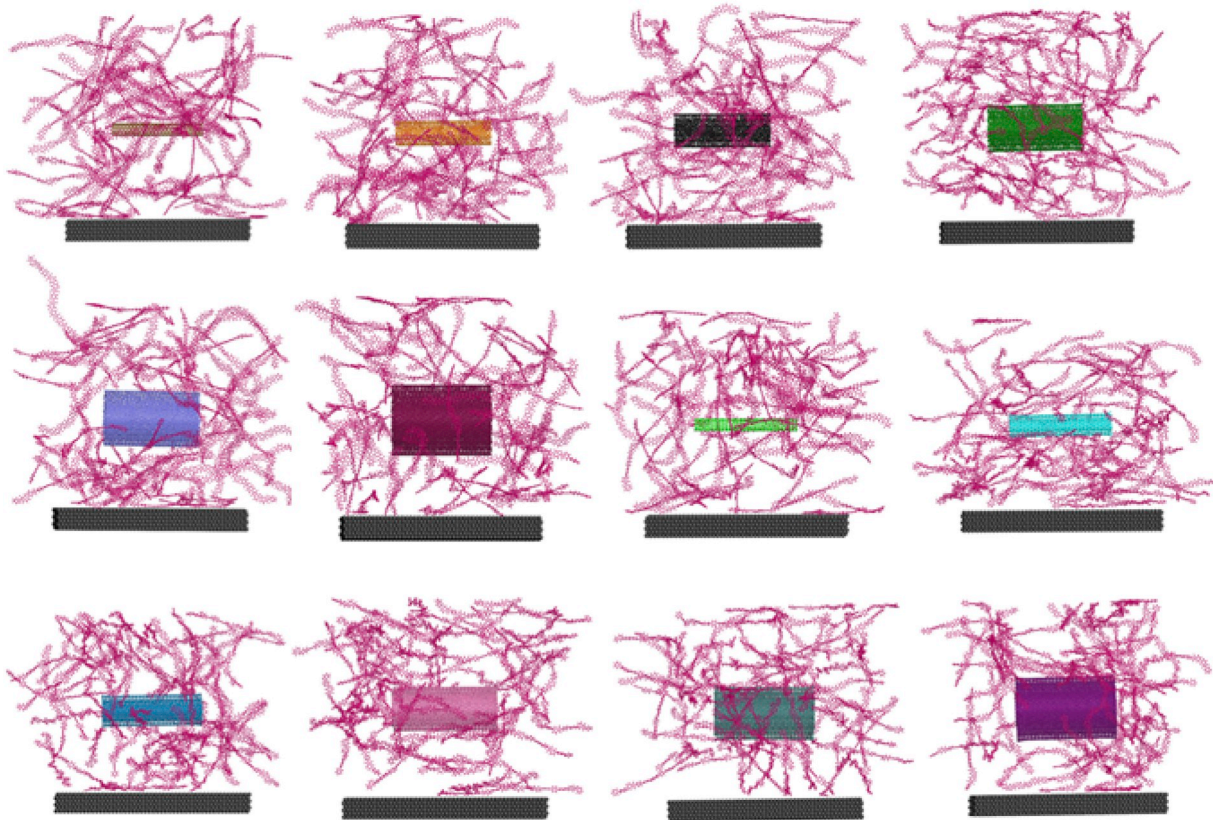
Fig. 3. Ti-PI-MWCNTs ternary system molecular dynamics simulation models.
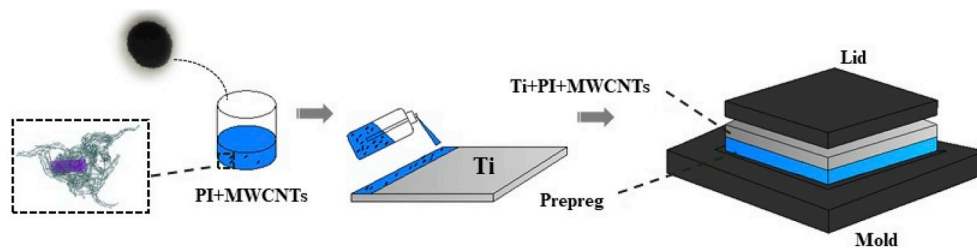
Fig. 4. The specimen preparation process.
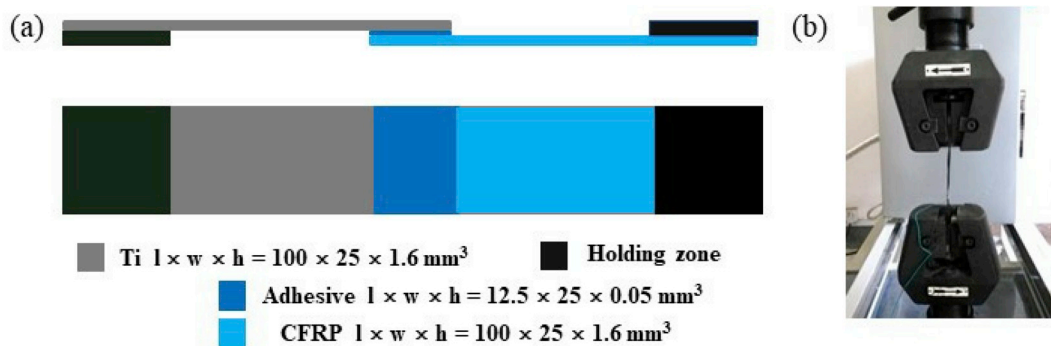
Fig. 5. (a) Represents the ILSS specimen; (b) The mechanical tests set up of ILSS test fixture.

types and wall numbers of CNTs were established. First, the structures of Ti, MWCNTs and PI were built in a cubic box (15 nm × 15 nm × 15 nm). A titanium layer was fixed in the bottom of the box. Four basic repeat units of PI illustrated in Fig. 1 were connected to make a polymer chain. Different types of 1–6 wall carbon nanotubes (CNTs) were established (Fig. 2) and placed along the X direction, parallel to the titanium. The wall separation distance (d) in CNTs was set to 0.35 nm, which is close to interlayer distance in graphite [20]. The open-end (6, 6) armchair MWCNTs were built to a length (L_{CNT}) of 6.13 nm and inner wall diameter (D) was 0.81 nm (as shown in Fig. 2(a)), the (10, 10) zigzag MWCNTs was built to a length (LCNT) of 6.39 nm and the inner wall

diameter was 0.78 nm (as shown in Fig. 2(b)). Next, PI molecules were filled the cubic box at weight ratio of 95 wt% where the MWCNTs was 5 wt% as shown in Fig. 3. For comparison, another case was filled 100 wt % PI molecules without MWCNTs.

Second, the MD simulation was conducted to analyze adsorption and shear behaviors of the interface. During building of the adsorption and shear model, single MWCNTs were added to the system, which could meet the needs of our research and reflect the overall phenomenon. Next, PI molecules were filled the cubic box at weight ratio of 95 wt% where the MWCNTs was 5 wt%. The angle between axis line of MWCNTs and horizontal X-axis of Ti was also controlled. The shear behavior was
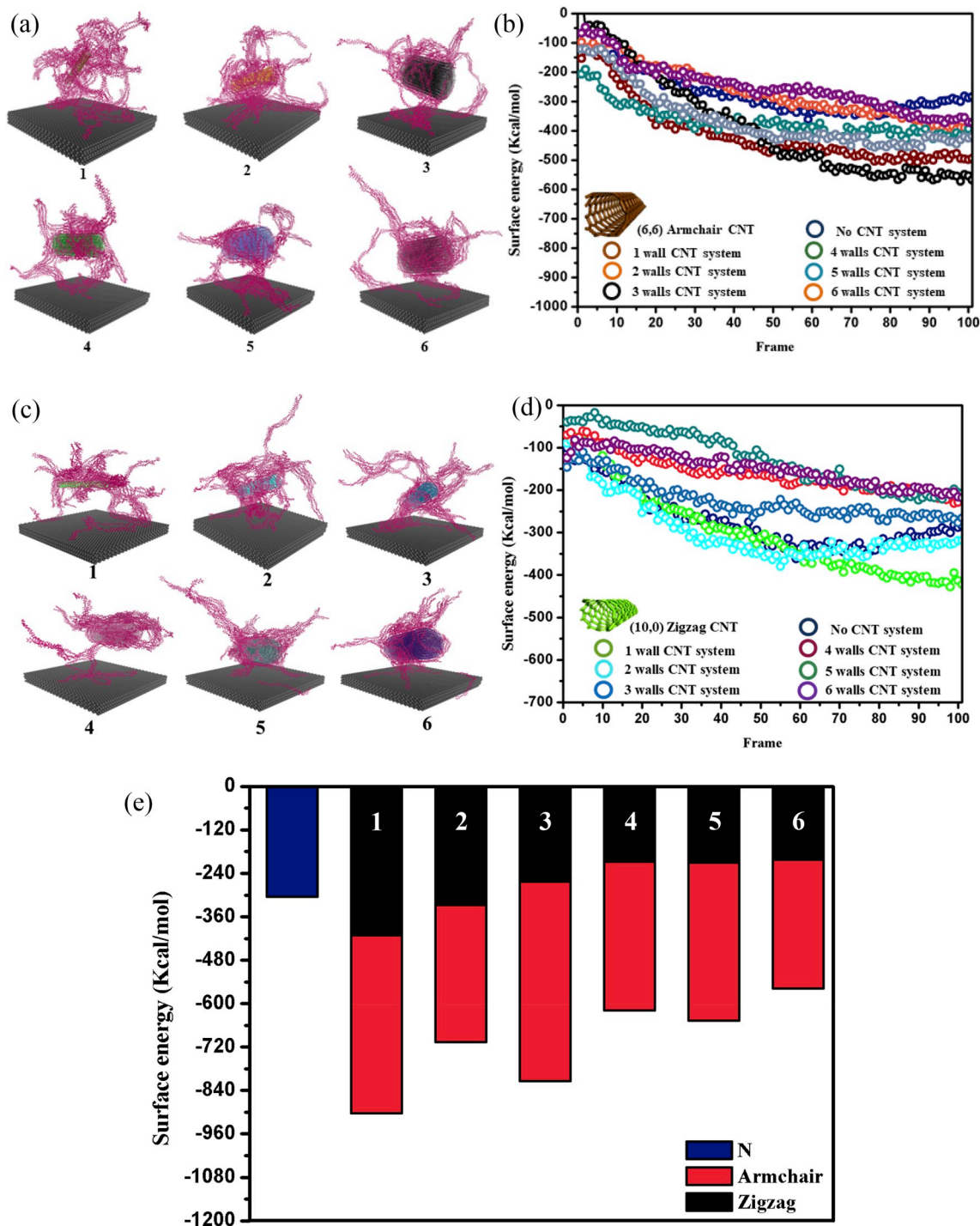
Fig. 6. (a) Final MD configuration of armchair type CNT; (b) Evolution of surface energy components of armchair type CNT system; (c) Final MD configuration of zigzag type CNT; (d) Evolution of surface energy components of zigzag type CNT system; (e) Average surface energy of the last 20 frames at different wall numbers.
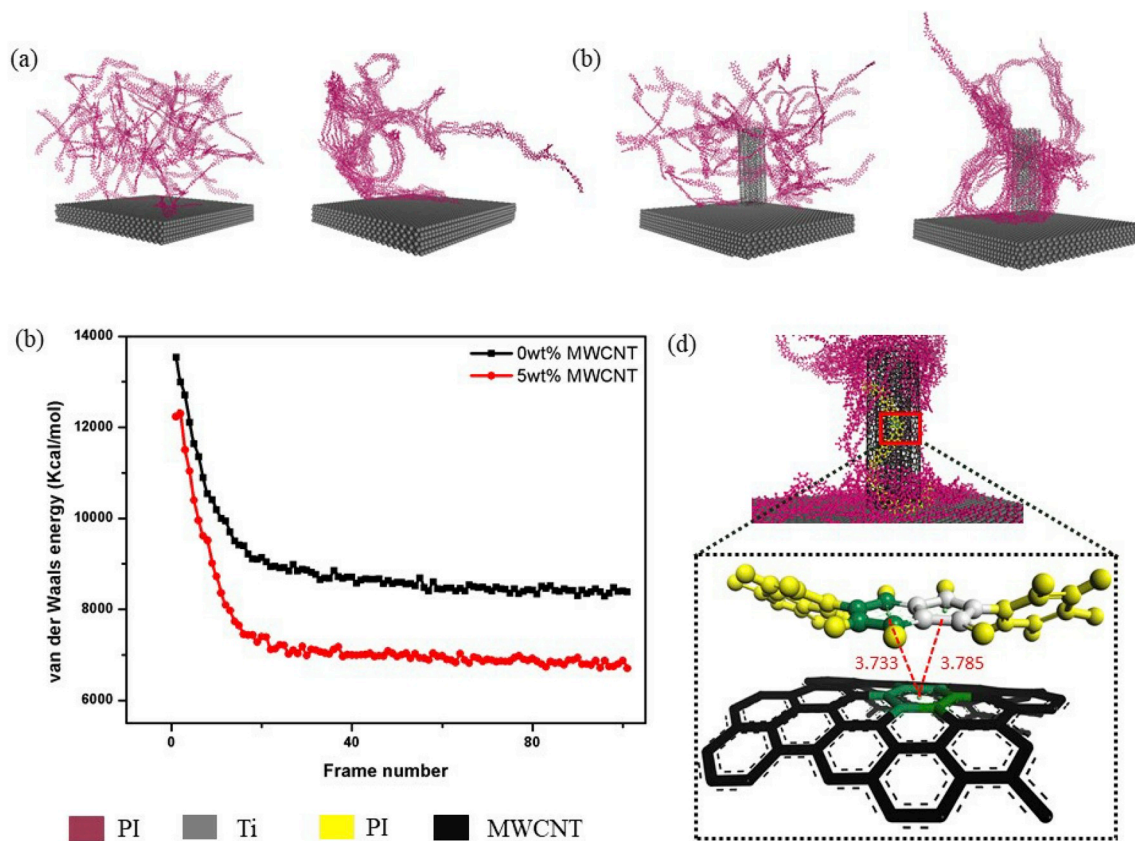
Fig. 7. (a) Molecular dynamic adsorption process of 0 wt% MWCNTs. (b) Molecular dynamic adsorption process of 5 wt% MWCNTs. (c) The evolution of vdW interaction energy of the system as a function of frame number. (d) The formed configuration of helix in MWCNTs.

simulated at 0.1/ps shear speed in 298K. The shear direction was set parallel to the Ti layer. The force-field of Dreiding [21] was applied to the atomic interaction model, which has been proved its applicability in describing interactions in complex mixtures [22,23]. The models were put into a canonical ensemble molecular dynamics (NVT-MD) simulation. The time step was set to 1.0fs. The result data were collected once every 5000ps to record a full-precision trajectory.

3. Macroscopic experimental

3.1. Specimen preparation

The specimen was composed of KH-308 polyimide matrix (provided by the Institute of Chemistry, Chinese Academy of Science), TA2 titanium plates (supplied by Baoji Yonshengtai Titanium Industry) and MWCNTs (came from Nanjing XFNANO Materials Tech.).

The preparation process is shown in Fig. 4. The first step was the dispersion of MWCNTs into polyimide resin matrix. An ultrasonic mixer (TJS-3000 Intelligent Ultrasonic Generator V6.0) was employed to disperse 5 wt% MWCNTs. The mixture was submerged in an ice bath to prevent overheating and reaggregation. The sonication conditions were set to 2 h sonication at half sonication amplitude [24]. The second step was the treatment of titanium sheet. The surface was treated by NaTESi anodizing process [6]. After that, the surface was painted with the mixture of PI and MWCNTs. Then, three treated titanium layers and two carbon fibre reinforced polyimide prepregs layers were stacked in sequence to construct unidirectional FMLs for single lap shear test. For the last step, the compression mold was put into the vulcanizing machine for curing and cooling [14]. Finally, test samples was cut by a diamond-tipped precision saw.

3.2. Single lap shear test

Single lap shear tests as shown in Fig. 5 were performed in accordance with ASTM D1002 standard at displacement rate of 2.0 mm/s and room temperature. The testing was stopped after adhesive joints failed and the force data were recorded. The maximum force (P_{max}) was used to calculate the interfacial fracture energy (G_E) of the Ti/CFRP using Eq. (4), derived from a model of shear stress-slip relation [25,26].
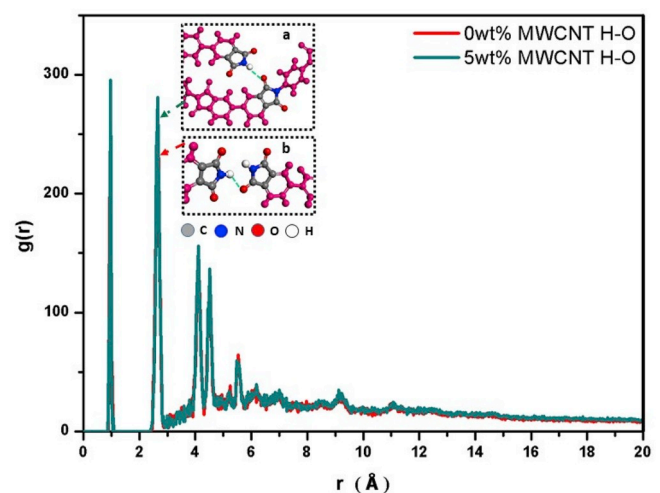
Fig. 8. RDF revolution between two reactive groups during adsorption process. The inset (a and b) shows the H bond in 5 wt% and 0 wt% MWCNTs systems.
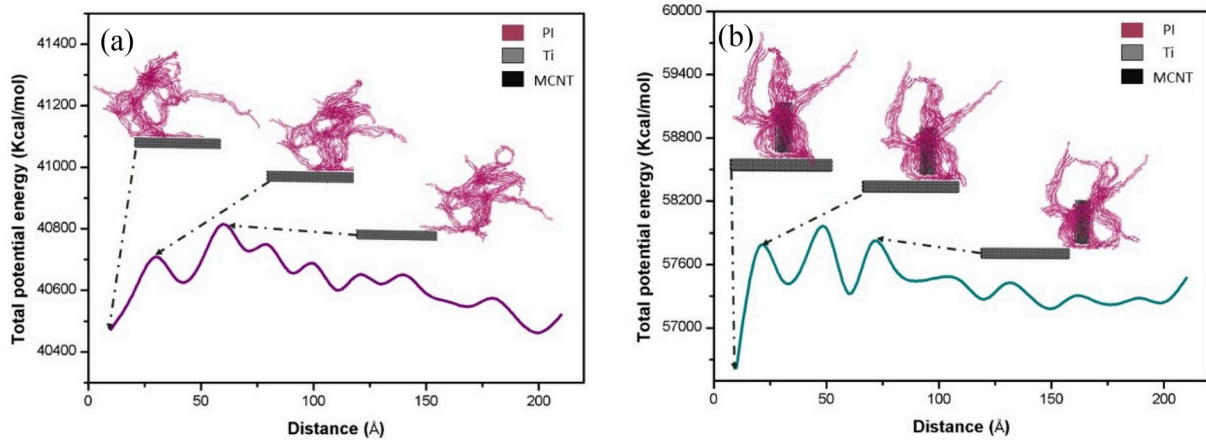
Fig. 9. Total potential energy during shear simulation: (a) 0 wt% MWCN and (b) 5 wt% MWCNT.

$$G_E = \frac{P_{max}^2}{E_{Ti}t_{Ti}b_{Ti}^2 + E_{CFRP}t_{CFRP}b_{CFRP}^2} \tag{4}$$

where, E_{Ti} denotes the elastic modulus of the Ti layer, t_{Ti} and b_{Ti} denote the thickness and width of the Ti layer. E_{CFRP} is the elastic modulus of the CFRP layer, t_{CFRP} and b_{CFRP} are the thickness and width of the CFRP layer.

The failure surface were characterized by field-emission scanning electron microscopy (FE-SEM, JEOL JSM 6700F) at emission current of 12 μA and accelerating voltage of 5 kV.

4. Results and discussions

4.1. Effect of MWCNT types on the interface performance

The effects of different types of CNT on the interfacial compatibility were shown in Fig. 6. The last frame trajectory conformations of the simulation are shown in Fig. 6 (a) and (c). It can be seen that the addition of different types of CNTs can significantly affect the morphology and contact area of the polyimide on the titanium surface. If adding the armchair CNT, the contact area of the PI on the titanium surface was
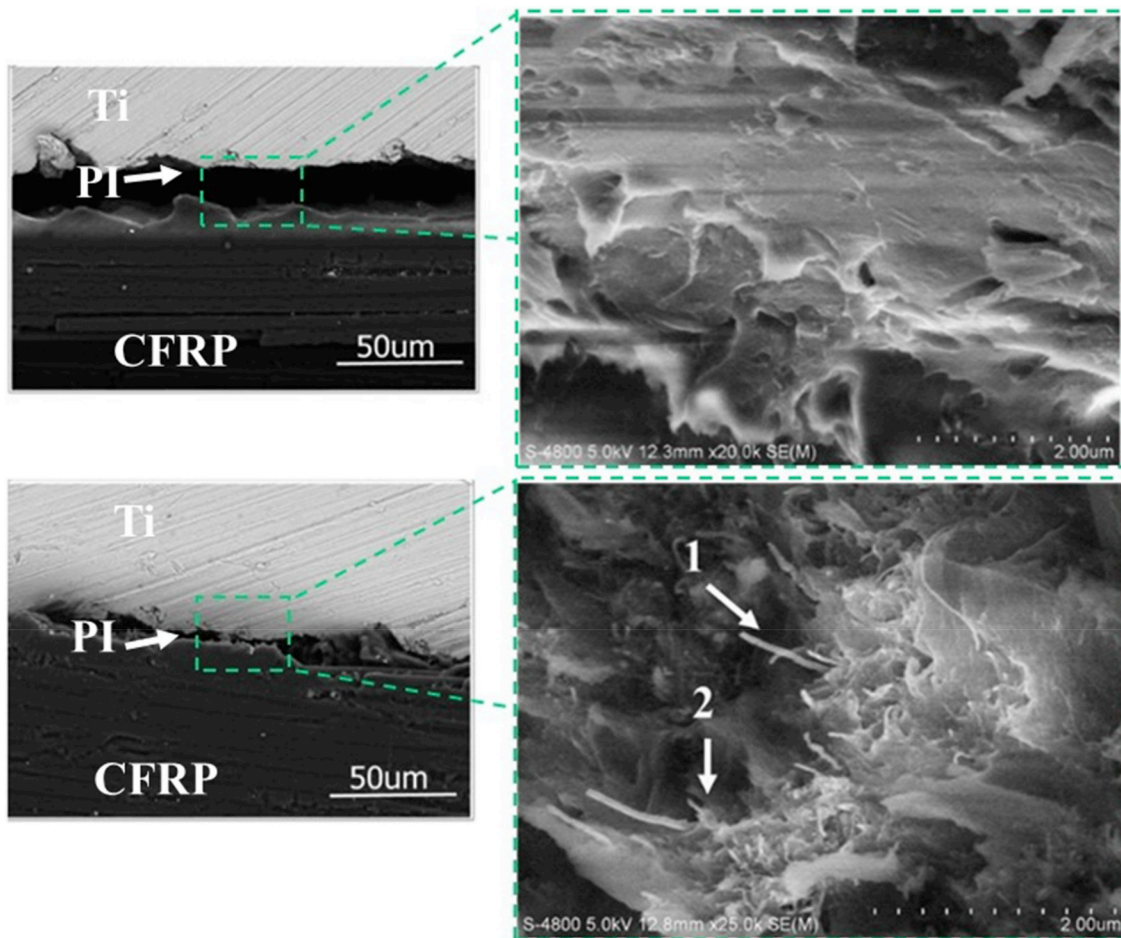
Fig. 10. Failure morphology of the interface: (a) 0 wt% MWCNTs; (b) 5 wt% MWCNTs.
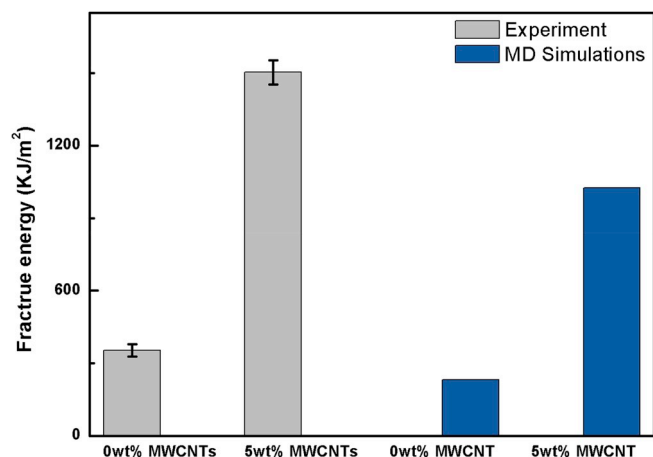
Fig. 11. Comparison of MD simulated fracture energy and experimental fracture energy.

larger than that of the added zigzag system. Fig. 6(b) and (d) are the evolution of surface energy of the armchair and zigzag CNT systems, respectively. It was found that different types of CNTs and the number of walls have a great influence on their interfacial properties. The armchair type CNT is better than the zigzag CNT for improving the interface performance (see Fig. 6(f)). The zigzag MWCNTs tended to decrease in interface enhancement with the increase of the number of tubes. When the number of walls was up to four, the system tended to be stable. The addition of zigzag CNT to PI has no obvious effect on the interface

enhancement. In the armchair CNT, when the number of walls was three, the surface energy is −551.1 kcal/mol. Compared with the system without CNTs, the interface effect was enhanced by 81.3%. Compared with the zaigzag system, the effect was also enhanced by 34.3%. If the number of walls exceeded three, the enhancement effect decreased. It can be found that the armchair three walled CNTs have the best interface enhancement effect. Beside, three walled CNTs have a good Young's modulus [27]. So the armchair three walled CNTs were used to analyze the reinforcement mechanism.

4.2. Mechanism of MWCNTs on the interface strengthening

In the MD simulation, only a few PI molecules were adsorbed on the Ti surface as Fig. 7(a) if no addition of MWCNTs. On the contrast, most PI molecules were adsorbed as Fig. 7(b) if adding MWCNTs. It can be seen from Fig. 7(c) that the van der Waals force reduced significantly when adding MWCNTs, which means the bonding strength was enhanced obviously. PI chains wrapped around the surface of MWCNTs (see Fig. 7(d)). The distances between the six rings in PI chain and five-membered centroid to the six-ring center of MWCNTs outermost wall were analyzed and determined as 3.733 Å and 3.785 Å. These should belong to the distance of π-π bond [28,29]. Therefore, it is concluded that the main adsorption driving force was the Van der Waals force. In addition, the chain was also driven to spirally distribute on the outermost walls of MWCNTs under the action of π-π bond surface.

The insert in Fig. 8 suggested that both systems had hydrogen bonds existing between H atom connected to N atom on the five rings of PI molecular chain and O atom on the five rings of the other PI molecular chain. The radial distribution function (RDF) g(r) could describe the
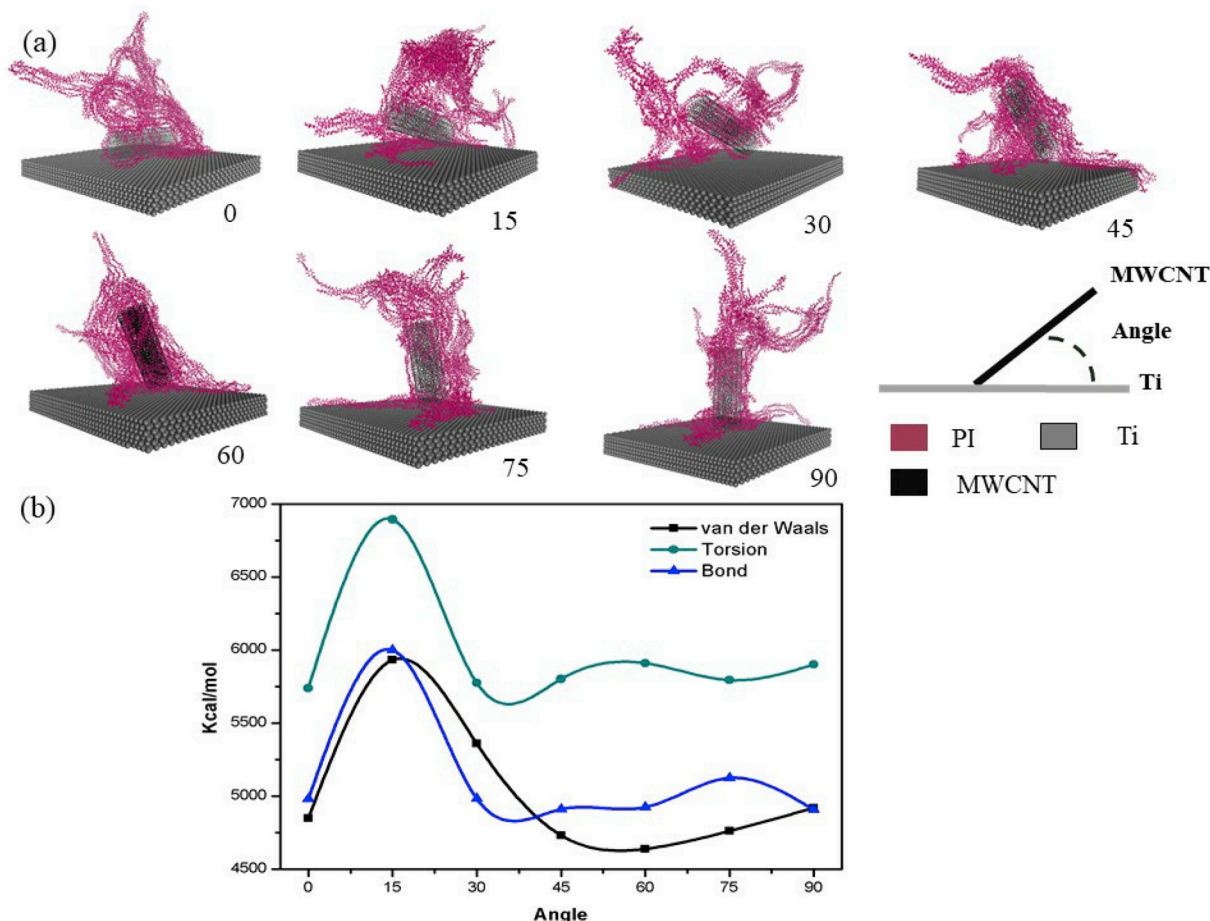
Fig. 12. (a) Final MD configuration at different angles. (b) Evolution of potential energy components during MD simulations.
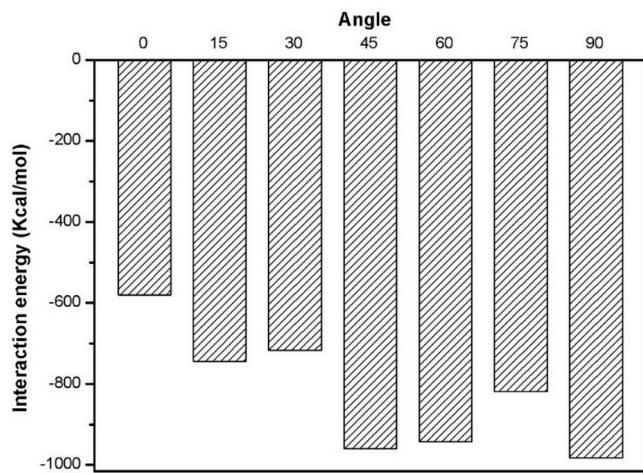
Fig. 13. Interaction energy between Ti and PI interface when MWCNTs are positioned at different angles from the Ti surfaces.

probability of existent pairwise atoms within certain distances in a system [30]. In this work, RDF was used to monitor the local structure evolution between two species of atoms, O and H atoms connected to N atom on the five rings of PI molecular chain during the adsorption process. For small distances, the RDFs of both systems shared the same peak position at approximately 1.0 Å, corresponding to the length of

chemical bonds between O and H atoms on five rings of PI molecular chain. The second peak represented a length of about 2.341 Å, mainly attributed to the distribution of hydrogen bonds formed by O and H atoms between each molecule. A peak zone evolution was also observed in the range $r > 2.5$ Å to $r < 12$ Å, mainly caused by mutual stacking of molecules.

The main attraction of PI molecules on MWCNTs and Ti surfaces were based on van der Waals forces. The PI molecules should be driven under the van der Waals forces to adsorb on the Ti layer and MWCNTs surfaces. The Van der Waals forces and hydrogen bonds were stacked with each other. In the Ti-PI-MWCNTs system, the PI molecules were adsorbed on the MWCNTs surface and distributed around the MWCNTs surface under the action of π-π bonding.

In both 0 wt% and 5 wt% MWCNTs systems (Fig. 9), the moving distances between the mass center of Ti surface and PI molecules on the Y-axis indicated the shear separation process between PI and Ti. The potential energy increased with the PI movement rising. In the 0 wt% MWCNTs system, the maximum potential energy was estimated to 40850 kcal/mol and minimum potential energy was 40490 kcal/mol. In the 5 wt% MWCNTs system, the maximum potential energy was recorded as 58100 kcal/mol and minimum potential energy was 56500 kcal/mol. According to Eq. (6), the fracture energy was calculated as 230.4 kJ/m^2 for the 0 wt% MWCNTs system and 1024 kJ/m^2 the 5 wt% MWCNTs system, respectively. On the other hand, The peak load (P_{max}) in shear test was 3250 N in the 0 wt% MWCNTs system and 1200 N in the 5 wt% MWCNTs system. By using Eq. (3), the fracture energies were calculated as 352.8 kJ/m^2 (0 wt% MWCNTs) for and 1504 kJ/m^2 (5 wt%
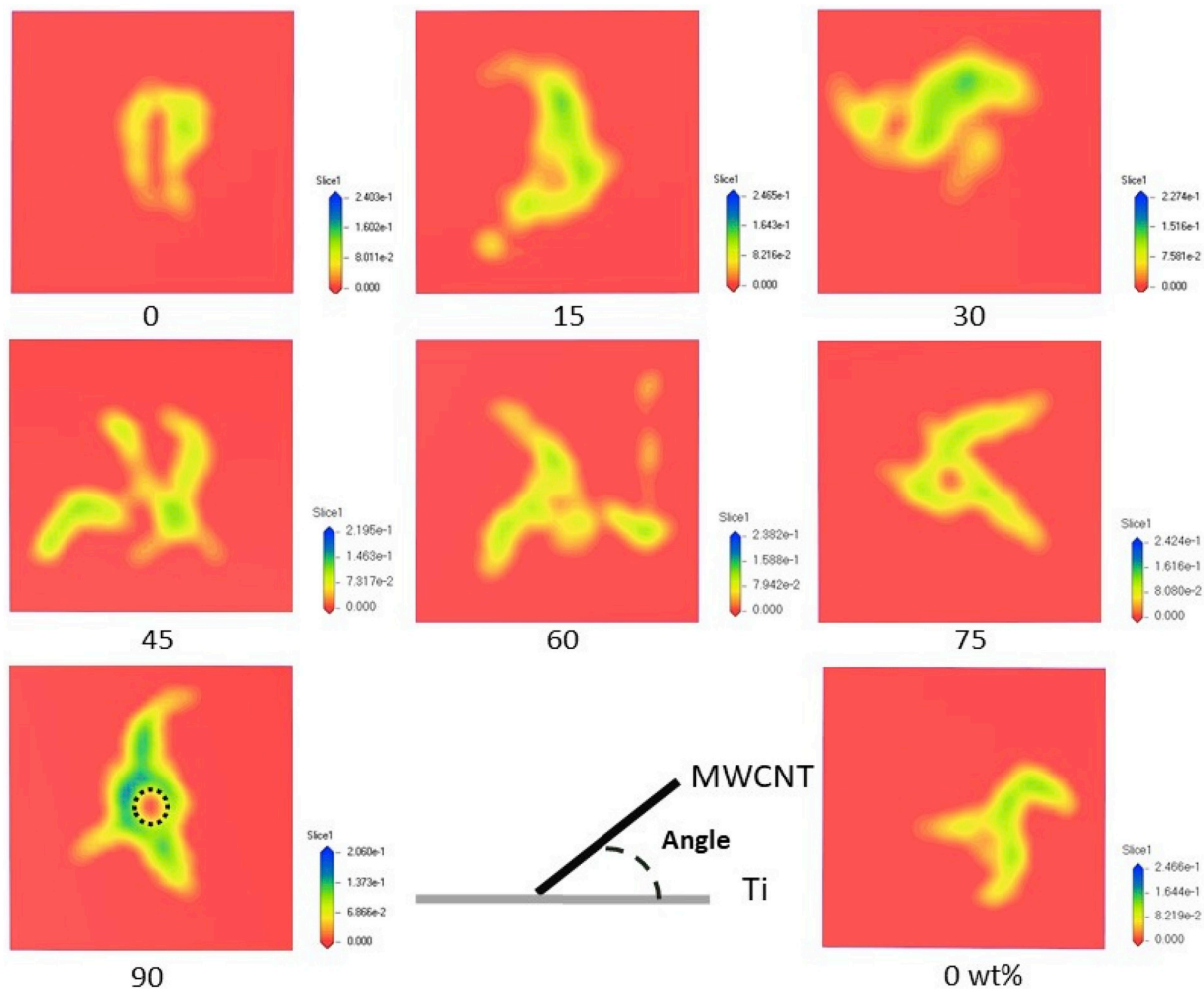
Fig. 14. The O atom density cloud map of PI molecules on Ti surface.

MWCNTs), respectively.

The addition of 5 wt% MWCNTs in PI resin showed positive effects on single lap shear behavior and increased shear strength by 87% when compared to that without addition of MWCNTs. The locus of failure shifted as shown in Fig. 10. The specimens without MWCNTs (Fig. 10(a)) were significantly delaminated with a large gap after suffering shear loading. In contrast, the gap of delamination is not very big (Fig. 10(b)) if adding MWCNTs into PI. Further observations showed that delamination of the specimen without MWCNTs occurred along the interface between Ti and PI. Ti surface was serrated and no resin adhered to the surface. Oppositely, the MWCNTs as a bridge connected the Ti and the PI resin. Regardless of MWCNTs pulled out or fractured (arrow 1 represents pulled out and arrow 2 represents fracture), the resin wrapped around the MWCNTs. MWCNTs surface-wrapped PI under stress conditions can disperse the buffer load [31], followed by MWCNT's own fracture, and pull-out failure consuming energy. Meanwhile, large numbers of fractured resin layers were attached to the surface of Ti and failure occurred along interior of the resin to yield cohesion. The addition of MWCNTs to the resin primer layer changed the failure mode. After addition of MWCNTs, the shear failure mode changed from interface failure to cohesive failure. The added MWCNTs improved shear resistance effectively.

The fracture energies of MD simulation and shear test were compared as listed in Fig. 11. Because of the treated rough surface of Ti sheet, there is a mechanical interlocking effect. However, the Ti surface in MD simulation was smooth. Therefore, experimental values were higher than simulation results but the trends were consistent. The fracture energy of the samples prepared with MWCNTs was five times higher than that of samples without MWCNTs.

4.3. Effect of MWCNTs orientation on the interface strengthening

The strengthening effect of MCWNTs has been proved in MD simulation when the axis of MCWNTs is perpendicular to the Ti surface. However, the effect of the orientation of MCWNTs on the interface strengthening has not been illuminated. To investigate the strengthening effect, seven different MCWNTs orientations (0°, 15°, 30°, 45°, 60°, 75°, 90°) were simulated.

As shown in Fig. 12, Ti layer surface with different MCWNTs orientations affected the molecular structure of the system and intermolecular interaction energy notably. The distribution and number of PI molecules on the Ti layer depended on the MCWNTs angles. Meanwhile, the number of absorbed PI molecules also varied by MCNTs angles. When the angles was 45° or 90°, the adsorption reached the maximum.

When MWCNTs were placed on Ti surface by angles, the interaction energies were calculated by Eq. (3) and the results are shown in Fig. 13. The difference of MWCNTs angles resulted in certain influence on the distribution and structure of PI molecules at the interface. When MWCNTs paralleled to the Ti layer, the interfacial interaction energy was the lowest. If MWCNTs were perpendicular to the Ti layer, the interfacial interaction energy became the highest. The O atom density cloud maps of PI molecules on Ti surface are shown in Fig. 14. In presence of MWCNTs, the effective contact area between PI molecules and TI was larger than that of the system prepared without MWCNTs. The distribution area of PI molecules on the Ti layer was relatively different when MWCNTs were positioned at different angles from the Ti surface. At 90°, the distribution area of PI molecular on Ti layer was larger than those obtained at the other angles. Therefore, the intermolecular interaction energy and the interfacial interaction strength were mainly affected by MWCNTs angles.

5. Conclusions

(1) To describe the interface behavior of the Ti-PI-MWCNTs, a ternary system was developed in MD analysis, including the interfacial interaction energy equations and ternary MD simulation models. The armchair type carbon tube has better effect on the interface compatibility than the zigzag type, and the 3 walls CNT was the best. It was found from MD analysis that a few PI moleculars were partially stacked and adsorbed on Ti layer and most PI molecules were adsorbed on the MWCNTs surface. The van der Waals force was the main driving force for adsorption of PI molecular. The PI molecules were entangled on MWCNTs surfaces under the action of π-π bond. Meanwhile, the presence of H–O hydrogen bonds promoted the absorption.

(2) It has been proved that the addition of MWCNTs to the PI resin matrix do improve the strength of Ti/CFRP interface. The MWCNTs as bridges can connect the Ti and the PI resin. No matter whether MWCNTs pull out or fracture, there were always some resins left on the MWCNTs and the Ti surface. The failure mode changed from interface failure to cohesive failure due to the addition of MWCNTs to the resin primer layer.

(3) When positioning MWCNTs at different orientations, the structure of the Ti-PI-MWCNTs ternary system was radically changed. The MWCNTs angle affected the adsorption form and quantity of PI molecules on the interface. The most PI molecules were present on the Ti layer surface at 90°, yielding best interface binding performance. On the contrary, if MWCNTs paralleled to the Ti layer, the interfacial interaction energy was the lowest, resulting in the minimum interfacial strength.

References

[1] Sharma Ankush P, Khan Sanan H, Parameswaran Venkitanarayanan. Experimental and numerical investigation on the uni-axial tensile response and failure of fiber metal laminates. Compos B Eng 2017:259–74.

[2] Hu YB, Li HG, Cai L, Zhu JP, Pan L, Xu J, et al. Preparation and properties of fibre–metal laminates based on carbon fibre reinforced PMR polyimide. Compos B Eng 2015;69:587–91.

[3] Hu YB, Zhang W, Jiang W, Cao L, Shen Y, Li HG, et al. Effects of exposure time and intensity on the shot peen forming characteristics of Ti/CFRP laminates. Compos Part A Appl Sci Manuf 2016;91:96–104.

[4] RV G, Cantwell WJ. The mechanical properties of fibre-metal laminates based on glass fibre reinforced polypropylene. Compos Sci Technol 2000;60(7):1085–94.

[5] Harris AF, Beevers A. The effects of grit-blasting on surface properties for adhesion. Int J Adhesion Adhes 1999;19(6):445–52.

[6] Xu J, Li H, Shen Y, Liu S, Wang W, Tao J. Improvement of adhesion performance between aluminum alloy sheet and epoxy based on anodizing technique. Int J Adhesion Adhes 2016;70:74–80.

[7] Liang CS, Lv ZF, Bo Y, Cui JY, Xu SA. Effect of modified polypropylene on the interfacial bonding of polymer–aluminum laminated films. Mater Des 2015;81: 141–8.

[8] He P, Chen K, Yang J. Surface modifications of Ti alloy with tunable hierarchical structures and chemistry for improved metal–polymer interface used in deepwater composite riser. Appl Surf Sci 2015;328(10):614–22.

[9] Gao HT, Yang X, Huang P, Xu KW. Enhancement mechanism of super fine machining pattern on mechanical property of adhesion interface of al alloy. Phy Proc 2013;50:288–92.

[10] Demczyk BG, Wang YM, Cumings J, Hetman M, Han W, Zettl A, Ritchie RO. Direct mechanical measurement of the tensile strength and elastic modulus of multiwalled carbon nanotubes. Mater Sci Eng, A 2002;334(1–2):173–8.

[11] Salvetat JP, Briggs GAD, Bonard JM, Bacsa RR, Kulik AJ, Stockli T, et al. Elastic and shear moduli of single-walled carbon nanotube ropes. Phys Rev Lett 1999;82 (5):944.

[12] Park C, Ounaies Z, Watson KA, Crooks RE, Smith Jr J, Lowther SE, et al. Dispersion of single wall carbon nanotubes by in situ polymerization under sonication. Chem Phys Lett 2002;364(3–4):303–8.

[13] Jiang Q, Li Y, Xie J, Sun J, Hui D, Qiu Y. Plasma functionalization of bucky paper and its Composite with phenylethynyl-terminated polyimide. Compos B Eng 2013; 45(1):1275–81.

[14] Zhang H, Gn SW, An J, Xiang Y, Yang JL. Impact behaviour of glares with MWCNT modified epoxy resins. Exp Mech 2014;54(1):83–93.

[15] García-Macías E, Guzmán CF, et al. Multiscale modeling of the elastic moduli of CNT-reinforced polymers and fitting of efficiency parameters for the use of the extended rule-of-mixtures. Compos B Eng 2019;159:114–31.

[16] Zhao JW, Song M. A computer simulation of stress transfer in carbon nanotube/polymer nanocomposites. Compos B Eng 2019;163:236–42.

[17] Tam LH, Zhou A, Yu Z, Qiu Q, Lau D. Understanding the effect of temperature on the interfacial behavior of CFRP-wood composite via molecular dynamics simulations. Compos B Eng 2017;109:227–37.

[18] Elkhateeb MG, Shin YC. Molecular dynamics-based cohesive zone representation of Ti6Al4V/TiC composite interface. Mater Des 2018;155:161–9.

[19] Li YL, Wang SJ, Arash B, Wang Q. A study on tribology of nitrile-butadiene rubber composites by incorporation of carbon nanotubes: molecular dynamics simulations. Carbon 2015;12:104.

[20] Li Y, Hu N, Yamamoto G, Wang Z, Hashida T, Asanuma H, et al. Molecular mechanics simulation of the sliding behavior between nested walls in a multi-walled carbon nanotube. Carbon 2010;48(10):2934–40.

[21] Mayo SL, Olafson BD, Goddard WA. Dreiding: a generic force field for molecular simulations. J Phys Chem 1990;94(26):8897–909.

[22] Lyu Q, Sun S, Li C, Hu S, Lin LC. Rational design of two-dimensional hydrocarbon polymer as ultrathin-film nanoporous membranes for water desalination. ACS Appl Mater Interfaces 2018;10(22):18778–86.

[23] Lunatriguero A, Vicentluna JM, Poursaeidesfahani A, Vlugt TJH, Sánchezdearmas R, Gómezálvarez P, et al. Improving olefin purification using metal organic frameworks with open metal sites. ACS Appl Mater Interfaces 2018; 10(19).

[24] Annu A, Singh A, Singh PK, Bhattacharya B. Effect of carbon nanotubes as dispersoid in polymer electrolyte matrix. J Mater Sci Mater Electron 2018:1–8.

[25] Gkikas G, Barkoula NM, Paipetis AS. Effect of dispersion conditions on the thermo-mechanical and toughness properties of multi walled carbon nanotubes-reinforced epoxy. Compos B Eng 2012;43(6):2697–705.

[26] Tam LH, Zhou A, Yu Z, et al. Understanding the effect of temperature on the interfacial behavior of CFRP-wood composite via molecular dynamics simulations. Compos B Eng 2017;109:227–37.

[27] Li CY, Chou TW. Elastic moduli of multi-walled carbon nanotubes and the effect of van der Waals forces. Compos Sci Technol 2003;63(11):1517–24.

[28] Lunatriguero A, Vicentluna JM, Poursaeidesfahani A, Vlugt TJH, Sánchezdearmas R, Gómezálvarez P, et al. Improving olefin purification using metal organic frameworks with open metal sites. ACS Appl Mater Interfaces 2018; 10(19).

[29] Główka ML, Martynowski D, Kozłowska K. Stacking of six-membered aromatic rings in crystals. J Mol Struct 1999;474(1):81–9.

[30] Yu B, Fu S, Wu Z, Bai H, Ning N, Fu Q. Molecular dynamics studies of interfacial crystallization behaviors in polyethylene/carbon nanotube composites. RSC Adv 2015;5(124):102219–27.

[31] Yuste SB, Santos A. Radial distribution function for sticky hard-core fluids. J Stat Phys 1993;72(3–4):703–20.